

Rockwell Hardness Testing on an Aluminum Specimen using Finite Element Analysis

Armin Yazdanshenas^{#1}, Chung-Hyun Goh^{#2}

[#]Department of Mechanical Engineering, the University of Texas at Tyler
3900 University Blvd., Tyler, TX 75799 USA

Abstract

Finite element analysis (FEA) has proven to be a convenient tool for many engineers in their respective fields. Its practicality and cost-effectiveness have also made FEA a routine prospect in the engineering industry. To give students a head-start in the early years of their professional careers, a basic understanding of FEA's fundamentals is prudent. This paper uses FEA to create a numerical simulation model of a real Rockwell hardness testing (RHT) on an aluminum specimen. A steel ball indenter and a total load of 60kgf are used according to scale H of the Rockwell hardness scale. The results of both the experimental and FEA case are compared to the theoretical Rockwell hardness of aluminum. In the experimental case, the percent error was approximately 5.56%. The FEA simulation provided results that fully matched the theoretical values.

Keywords—Finite element analysis, Rockwell hardness testing, Explicit dynamic simulation

I. INTRODUCTION

A. Background

Hardness is a mechanical property that indicates a material's resistance to localized plastic deformation caused by a mechanical indentation. In engineering, hardness is mainly used for the determination of material properties of various materials. In solid mechanics, the investigation of hardness in materials is generally reduced to and focused on metals and their mechanical behavior. To understand the mechanism behind hardness in metallic structures, a basic understanding of materials science is needed. Since a metal's properties are directly related to its microstructure, defects in a specimen's microstructure affect the hardness. Line defects, such as dislocations along planes in the crystal lattice, cause atoms' planes to slip, which results in permanent deformation. The more susceptible a metal's microstructure is to the plastic deformation caused by dislocations, the lower the hardness will be. On the other hand, intersections of two or more dislocations can create an anchor point that prevents further slippage along the planes [1].

The ascertainment of a material's hardness may be performed through several different testing methods: Brinell, Rockwell, Vickers, or Knoop hardness test. All of these tests reference common terminologies and basic procedures. For example, the material sample under investigation is called the specimen, and the testing component responsible for inducing the indentation to the specimen is referred to as the indenter. In the Brinell hardness test, a 10mm diameter carbide or hardened steel ball is generally used as the indenter. Applying a controlled force of up to 3,000kgf to the specimen for 10s to 15s leaves a permanent dome-like depression onto the specimen's surface. Measurements of the resulting imprint are used to determine the Brinell Hardness Number [2] [3]. The Knoop hardness test is a reduced version of the Brinell hardness test; one of the main differences is that the test specimens are downsized material features. Therefore, a maximum testing load of 1kgf is used. Because this test is performed on a micro scale, all measurements must be made with diligent precision to retrieve the Knoop Hardness Number [4]. Another key distinction is that a rhombus-shaped indenter makes the depression onto the specimen's surface. The Vickers hardness test is a happy medium between the two previously mentioned hardness tests, tackling both the macro and micro hardness scales. With applied loads ranging anywhere from 1kgf to 100kgf, this hardness test utilizes the vertex point of the diamond side of a square pyramid indenter to puncture the specimens. Analysis of the indentation is used to calculate the Vickers Hardness Number [5] [6] [7].

Rockwell hardness testing (RHT) is slightly different from the previously mentioned hardness tests. Although the fundamentals remain the same, the procedures conducted in RHT are more systematic so that measurements are made quickly, easily, and with excellent reproducibility [8]. Test machines for RHT are also user friendly; the hardness number can be read directly from a dial, as shown in Fig. 1.



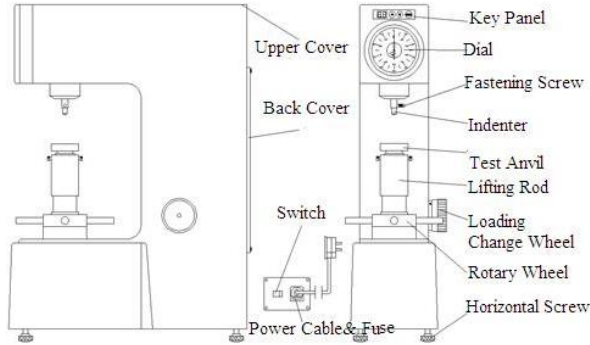


Fig1: Rockwell Hardness Test Machine Schematic [9]

RHT uses the Rockwell scale, shown in Table 1, to denote different loads, indenters, typical applications, and other such parameters. Since it is necessary to indicate which indenter and forces have been employed during RHT, a Rockwell hardness number is always followed by symbols representing the test's parameters. In RHT, the Rockwell hardness number is always followed by the symbol HR and scale designation symbol. If a ball indenter is used, the scale designation symbol is followed by the letter *W* to indicate a tungsten carbide ball or *S* to indicate a steel ball. For example, 75 *HRA* equates to a Rockwell hardness number of 75 on the Rockwell scale *A*. Likewise, 51 *HRBS* equates to a Rockwell hardness number of 51 on the Rockwell scale *B* using a steel ball indenter.

B. Goal & Objectives

This report aims to study the fundamentals of elastic material properties as a constituent element of mechanical engineering. Modern engineering tools and techniques common to the engineering industry will be applied to assess this study's findings and reinforce engineering problem-solving.

This report's main objective is to demonstrate the empirical formulation of aluminum's hardness through RHT as outlined in ASTM E18 and ISO 6508-1. RHT will be conducted on an aluminum specimen as part of the experimental portion of this study. Finite element analysis (FEA) will be used to provide a second perspective on the hardness property of the aluminum specimen. The RHT results and FEA solution will be compared to each other and the actual hardness properties of aluminum, as indicated by empirical data.

C. Tasks

1. Perform RHT of scale H on an aluminum specimen using a Rockwell hardness test machine
2. Recreate RHT of scale H numerically using FEA simulation to extract permanent deflection induced by the indenter and the major load

3. Calculate and compare both the experimental and FEA cases' hardness values to each other and empirically tabulated data.

II. LITERATURE REVIEW

A. Hardness in Academia

Hardness testing is a common topic found in the current literature. One such topic involves the improvement of RHT and its overall accuracy through new calibration methods. One of these methods involves the establishment of a multi-indenter group standard for calibration. Rather than using a single indenter to calibrate the Rockwell testing machine, a standardized group of indenters is used to enhance the calibration process [11]. As expected, the multi-calibration approach eliminates uncertainties by extracting far more calibration data points than is possible with a single indenter. The second calibration improvement method corrects RHT hardness values by computing the indenters' area function with the use of a highly accurate stylus profilometer[11]. 3D scanning coupled with homodyne laser interferometers offers direct measurement traceability of the indenter's displacements. Radial scanning of the indenter's tip also allows for the design of a special radial scan function. With this, the area function of any indenter may be found from its 3D geometry.

**TABLE I
ROCKWELL HARDNESS SCALES [10]**

Scale	Indenter (in)	Force (kgf)	Dial Figures	Application
B	1/16 ball	100	red	copper alloys, soft steels, aluminum alloys
C	diamond	150	black	steel, hard cast irons, titanium
A	diamond	60	black	cemented carbides, thin steel, and shallow case-hardened steel
D	diamond	100	black	thin steel and medium case-hardened steel, pearlitic malleable iron
E	1/8 ball	100	red	cast iron, aluminum, or magnesium alloys, bearing metals
F	1/16 ball	60	red	annealed copper alloys, thin, soft sheet metals
G	1/16 ball	150	red	malleable irons, copper-nickel-zinc, and cupro-nickel alloys
H	1/8 ball	60	red	aluminum, zinc, lead

Researchers in academia have also attempted to determine the dislocation densities of certain metals using hardness measurements. The hardness indentation size demonstrated that multi-pass friction stirs processed metal had much lower dislocation

densities than its single-pass counterparts [12]. The results on the metals' tensile properties indicated that the multi-pass friction stir processed metal had greater changes in its tensile behavior than did the single-pass friction stir processed metal. Analysis of both metal processes' true stress versus true strain graphs proved that a two-pass progression experienced yield drop at high strain rates.

Hardness analysis has also been used to investigate the microstructural behavior of new composite materials. Depending on the aluminum powder weight percent composition and the milling time, the graphene-nanoplatelets/aluminum composites' mechanical properties differ. Once synthesized through mechanical alloying, the test composites were prepared for Vickers micro-hardness tests to characterize their hardness behavior. Based on the hardness test results, homogeneous dispersion of graphene, and proper selection of sintering conditions were considered to optimize and revamp the composites [13]. Many other applications of hardness testing for the determination of material properties exist in the current literature. For instance, mechanistic analysis of the correlation between material strength and hardness has been developed for discontinuously reinforced aluminum [14]. Methods have also been developed to test for hardness properties of steel without destroying the test specimen [15]. In general, advancements and innovation in hardness testing are abundant in academia.

B. Finite Element Method

Many of the research topics mentioned in the previous section have also been investigated using computer simulation approaches. For instance, the Vickers, Brinell, and Rockwell hardness tests have all been performed in the virtual platform. Using FEA, a new approach has been presented for the Vickers hardness test's finite element modeling. Researchers have also developed a numerical correlation between the modulus of elasticity and hardness using the finite element method [16]. Even though methods for determining mechanical properties of materials have been around for a long time, some property was deriving tests, such as the Brinell and Rockwell hardness tests, still lacking insight for effective quality control. This is mainly due to the intricate deformation processes that occur during indenter puncture. However, researchers have successfully recreated the complexities of time-varying stress-strain states in FEA to accurately model and simulate the Brinell and Rockwell hardness tests [17].

FEA is also a commonhold for simulating hardness properties of complex composites, structures, and microstructures. In one study, carbon nanotubes-doped diamond-like carbon film was used to determine the

optimal nanotube orientation for best hardness values [18]. Using the nanoindentation hardness theory, 2D and 3D finite element models of the carbon nanotubes were built incongruence. Hardness behavior analysis was conducted on the carbon nanotubes at different orientations. From the finite element model results, the hardness of carbon nanotubes-doped diamond-like carbon/silicon composites was directly dependent on the orientation and volume fraction of the carbon nanotubes. In other research papers, this work was extended over to Al 1080/Si-C particle reinforced metal matrix composites. Using non-linear FEA, the equivalent stress and strain distributions, and the indentation depths were compared to experimental results [19]. According to the research, as the volume fraction of reinforcement decreased and the particle size of reinforcement increased, the indenter's puncture depth was also increased. As a result, the hardness was ultimately decreased.

III. METHODOLOGY

A. The Rockwell Hardness Test

A diamond cone or hardened steel ball indenter is used to indent the specimen with a preliminary (minor) load. Once equilibrium has been reached, the indenter's depth penetrates the specimen is recorded and used as the reference position (datum). With the minor load still active, an additional (major) load is imposed onto the indenter's specimen. The total load (minor plus major load) causes an increase in the penetration depth. Once equilibrium has been reached again, the major load is removed while still maintaining the minor load. Upon removing the major load, the penetration depth undergoes partial elastic recovery. Figure 2 illustrates this process. The difference between the final penetration depth and datum is the permanent deformation incurred by the specimen due to the application and removal of the major load. Using Eq. (1), the Rockwell hardness number, RHN , can then be calculated

$$RHN = E - \frac{h}{0.002 \text{ mm}} \quad (1)$$

where E is a constant depending on the form of the indenter (100 for diamond indenter and 130 for steel ball indenter), and h is the permanent increase in depth of penetration due to the major load [10]. RHN is an arbitrary number that indicates the material specimen; the higher the value of RHN , the harder the material. Reciprocally, the smaller the value of RHN , the lower the hardness.

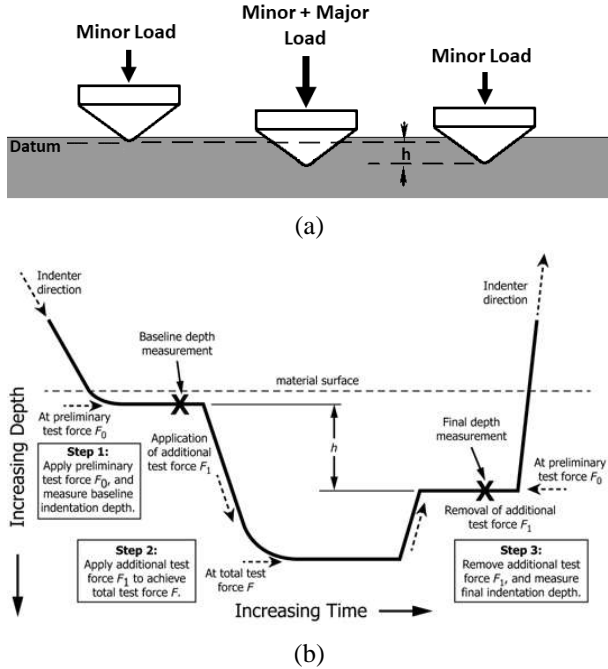


Fig 2: Rockwell Hardness Test (a) Physical Schematic [20] (b) Graphical Schematic [10]

B. Experimental Setup

In the experiment, an aluminum specimen with a length of 1.5 in., a width of 1 in., and thickness of 0.25 in. was prepared. Making sure that the specimen was free of blemishes, notches, cuts, and other deformities, the aluminum piece was placed on the test anvil, an RHT machine. A 1/8 in. diameter ball indenter was fastened to the testing machine using the fastener screws, and the center of the aluminum specimen's surface was aligned with the indenter. As prescribed by scale H of the Rockwell hardness scale, a 10kgf minor load was applied to the specimen by the indenter with about 3s in dwell time. Using the loading change wheel of the testing apparatus, the major load was added so that a total load of 60kgf was being applied to the specimen. At this point, the total load was maintained on the specimen for an estimate of 10s. Longer dwell time was used to ensure that all of the deformations introduced by the additional load had settled as much as possible. By reversing the loading change wheel to its initial position, the major load was removed while maintaining a constant minor load of 10kgf. Courtesy of the built-in processes of the testing apparatus, the resulting RHN of the test was displayed on the dial of the RHT machine. After recording the RHN of the experiment, Task 1 had been completed.

C. Finite Element Simulation

The experiment outlined in the previous section was recreated in ANSYS. To represent the RHT as an FEA

model as efficiently as possible, the ball indenter and aluminum specimen geometry were reduced using symmetry. In doing so, the FEA simulation can be shaped such that the computer's processing power and memory are not used unnecessarily, especially when symmetrical simplifications are available. By reducing the size of the ball indenter into an eighth of a sphere and shrinking the size of the specimen so that it is just big enough to account for the puncture as shown in Fig. 3, the FEA simulation is capable of performing its analysis on a smaller geometry without losing any information vital to the solution of the simulation.

In the geometry, the one-eighth piece of the indenter was given a 1/16 in. Radius. The dimensions of the specimen were reduced arbitrarily to the diameter of the ball indenter: 1/8 × 1/8 × 1/8 in.³. Material properties were also assigned at this stage of the FEA simulation; steel was assigned to the specimen's indenter and aluminum. Since the indenter is technically not part of the analysis, it could be argued that perfect rigidity may be applied to the indenter so that the simulation may be reduced and simplified even further. Even though the deformation in the steel is much smaller than the expected deformations of the aluminum specimen, removing the steel indenter's behavior would exclude the small differences that the elastic properties of steel would bring the simulation. Moreover, RHT deals with changes in extremely small deflections, making it imperative to include all physical factors.

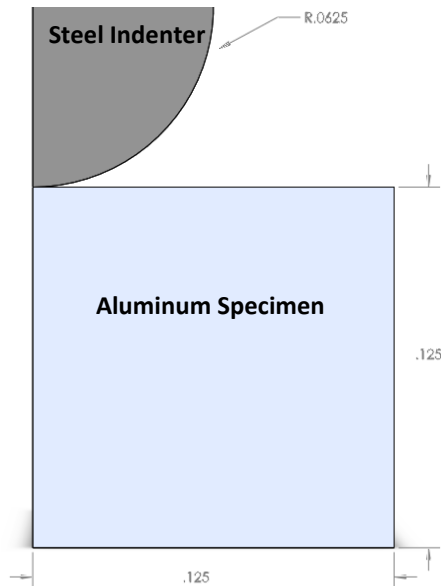


Fig 3: Side View of Model Geometry View (units in inches)

As for the mesh, a maximum element size of 2 mm was parameterized for the entire model mesh. Since the region of interest lies on the specimen at the point of

contact with the indenter, mesh refinement was applied to increase the mesh's details at the point of contact. Using ANSYS's inflation function, the mesh was refined radially on the aluminum specimen. With an inflation radius of 1 mm, the maximum element size of all elements within 1 mm of the contact point was reduced to 0.1 mm. Figure 4 demonstrates the resulting mesh configuration on the aluminum specimen. Mesh refinement on the indenter was not considered due to the lack of interest in the deflections that occur to it, so a maximum element size of 2 mm was applied to the steel indenter. Overall, the total number of nodes and elements used in meshing the model was 6,000 and 30,000, respectively.

Figure 5 shows the boundary conditions used in the FEA simulation. Symmetric boundaries were applied to the surfaces of the model, where the symmetric cuts were made. Colored yellow in Fig. 5, the symmetric boundaries work by preventing any displacements from going into or coming out of the surface plane. In this manner, the nodes and elements can only shift along the surface plane as if they were an internal part of a larger model.

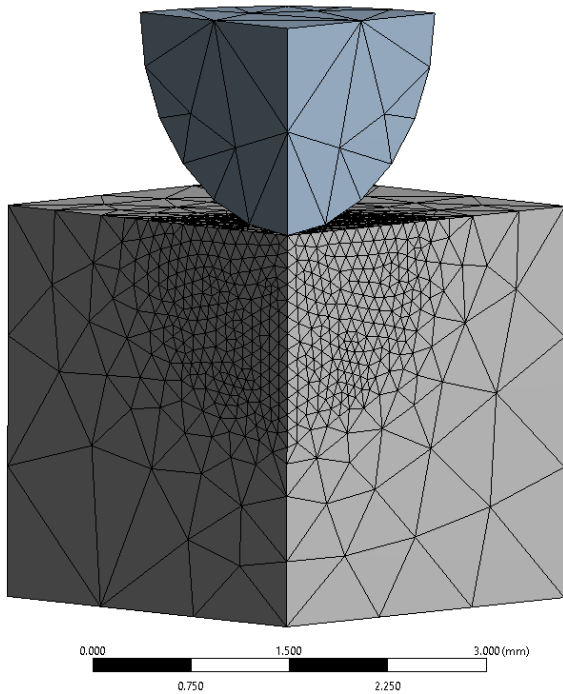


Fig 4: Mesh Refinement at Point of Contact

The reaction forces resulting from the test anvil's support are represented by a fully-fixed boundary condition colored blue in Fig. 5. Located at the bottom of the specimen, the fully-fixed support accounts for the normal forces and frictional forces, keeping the specimen from moving and slipping off the test anvil. In

the FEA simulation, the fully-fixed support ensures that all displacements, velocities, and accelerations of the surface are nullified. However, any forces needed to keep the bounded surface in static equilibrium are automatically calculated and applied by ANSYS.

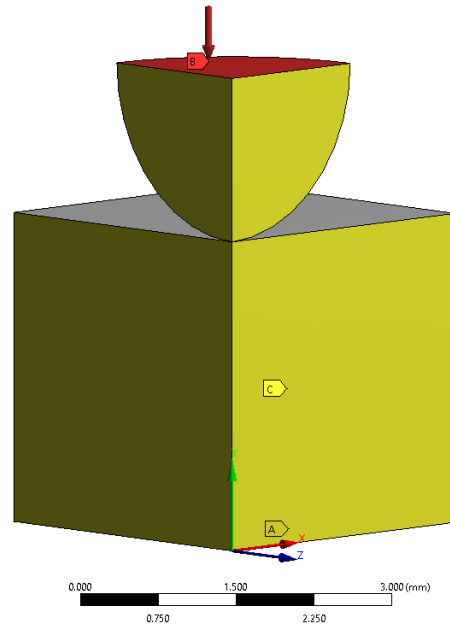
The minor, major, and total loads of the indenter are recreated in the FEA simulation as pressure loads applied to the top surface of the indenter, as shown in red in Fig. 5. To convert the force exerted by the 10kgf minor load and 60kgf total load into a pressure load, the magnitude of the forces was divided by the total area of the red surface. With this, the forces are distributed evenly over the indenter's top surface, equivalent to how a pressure load is applied. Applying the pressure load to the one-eighth indenter model's top surface allows for a more realistic specimen-indenter interaction; changes in both the indenter and specimen are accounted for.

All other surfaces are left as free surfaces that behave freely and naturally in response to the surrounding nodes and elements' changes. Once all of the boundary conditions were set, the simulation was run to mark Task 2.

A: Explicit Dynamics

Pressure
Time: 5.e-005 s
4/21/2019 11:04 PM

- Fixed Support
- Pressure: 297.27 MPa
- Displacement 2



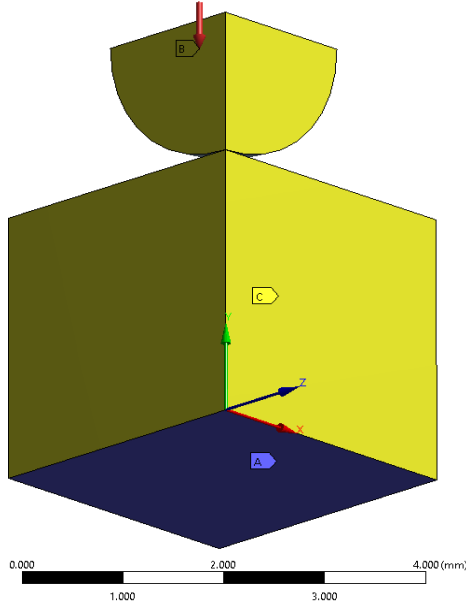


Fig 5: Applied Loads and Boundary Conditions

IV. RESULTS& DISCUSSION

A. Experimental Results

The resulting indentation of the RHT physical experiment is shown in Fig. 6. The close-up in Fig. 6 (b) clearly shows the imprint left by the steel ball indenter on the aluminum specimen's surface. Due to the limited precision of the measuring instruments made available, reliable measurement of the indentation depth could be made directly. Unreliable measurements are also a result of the protuberances that form on the indentation's edge. However, estimations of the puncture depth were made by directly measuring the diameter of the hole. The hole diameter was measured with a caliper, resulting in an average diameter of about 0.129 in. The indentation depth was assumed to be one radius in length or half of the hole diameter. Therefore, indirect measurements of the indentation depth result in an estimated depth of 0.0645 in.

Unfortunately, even with the estimation of the indentation depth, the indentation depth of the datum when the minor load was first applied is also required to calculate the *RHN* with Eq. (1). Since the testing apparatus used in the experiment works so that the datum depth cannot be measured once the test has started, the *RHN* cannot be calculated by hand. However, as stated in the previous sections, the testing apparatus automatically displays the *RHN* on a dial. Using the *RHN* indicated by the testing apparatus, the aluminum specimen has a *RHN* on scale H of 102 *HRHS*.

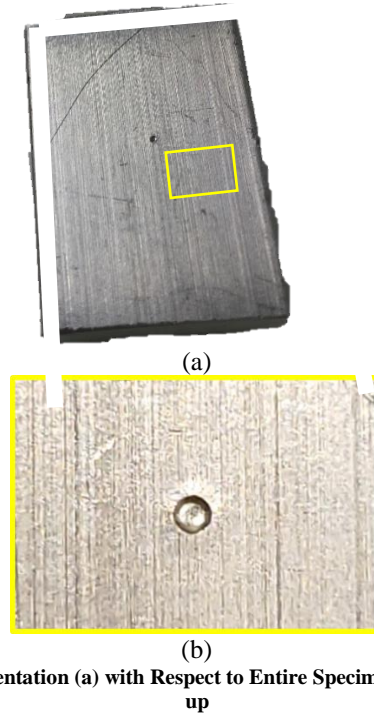


Fig 6: Indentation (a) with Respect to Entire Specimen (b) Close-up

B. Finite Element Solution

Figures 7-9 illustrate the displacement of the aluminum specimen throughout the RHT process as determined by the explicit dynamic simulations. Due to the extremely high relative deformations experienced by some of the elements directly underneath the indenter, those elements were considered broken-off from the specimen and excluded from the color bar results. For this reason, the color bars on the left-hand side of Figures 7-9 all depict smaller deflections than what was calculated. Fortunately, ANSYS's probe function can be used to probe the actual maximum deflection calculated by the FEA simulation. The maximum deflections are depicted in the expanded turquoise boxes.

Figure 7 portrayed the aluminum specimen's deflection when the minor load was applied in the initial stage of the RHT. Using a true scale, the specimen model's actual deformations are illustrated in the isometric and side views. In the side view, the change in the slope of the specimen model's surface can be observed. Since a ball indenter was used, the specimen model's deformation profile assumed the shape of the incoming indenter, causing large deformations at the point of contact and gradually smaller deformations further away from the point of contact. Due to the indenter's spherical nature, this is true for all radial directions; however, the downward direction of the applied load significantly adds to the vertical deformations.

In terms of deflection, the specimen endured the largest deflections exactly at the initial point of contact. This is expected since the ball indenter exerts a majority of the

minor load at this point. As the ball indenter continuous to push against and puncture through the aluminum specimen, the contact area between the two gradually increases, causing the 10kgf minor load to be distributed over the growing contact surface. As a result, the increased contact surface area causes the induced pressure to decrease. The pressure continues to decrease until the force applied by the minor load equals the specimen's reaction force. Once static equilibrium is reached, the indenter ceases to penetrate the specimen any further, marking the data's depth. According to the explicit dynamic FEA simulation solution, the maximum deflection of the minor load at the initial stage was 0.061645 mm in the downward direction, as shown in Fig. 7. This value will be used as the datum and for part of the calculation of the permanent deflection.

case, the total load causes the specimen to deform and deflect in greater magnitudes. This is shown by the larger red areas in Fig 8. Visual inspection of the aluminum specimen's isometric and side views reveals much greater deformations occurring directly underneath the steel indenter. As is expected, the applied load increase causes the ball indenter to penetrate deeper into the specimen. Similarly, the pressure of the minor load decreased with increasing contact surface area. The pressure induced by the total load slowly decreases as the indenter comes in greater contact with the specimen. The only difference, in this case, is that the reaction forces of the specimen require more contact area to counter the much larger 60kgf total load. With the total load in place, the maximum deflection was 0.14188 mm in the downwards direction. Again, the probe function was utilized to extract the maximum deflection location and value.

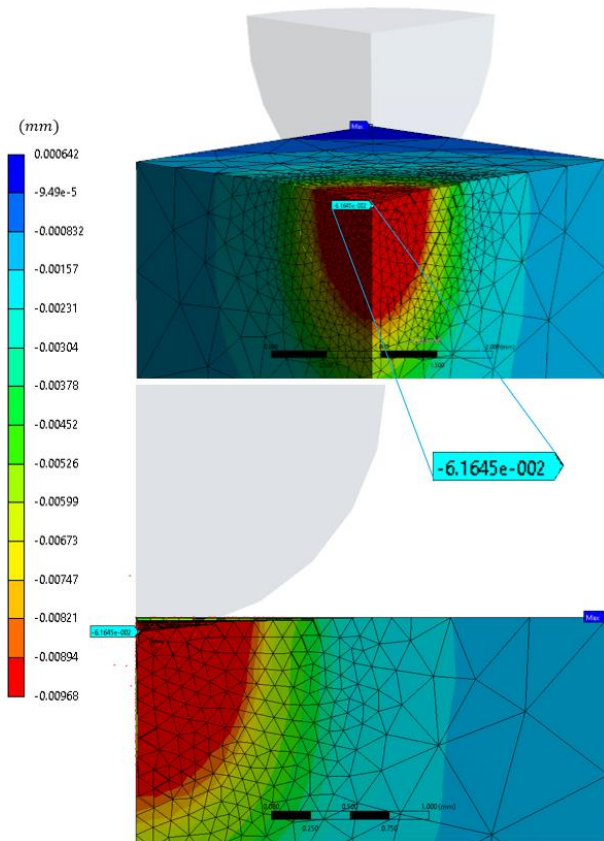


Fig 7: Deflection Due to Minor Load (10kgf)

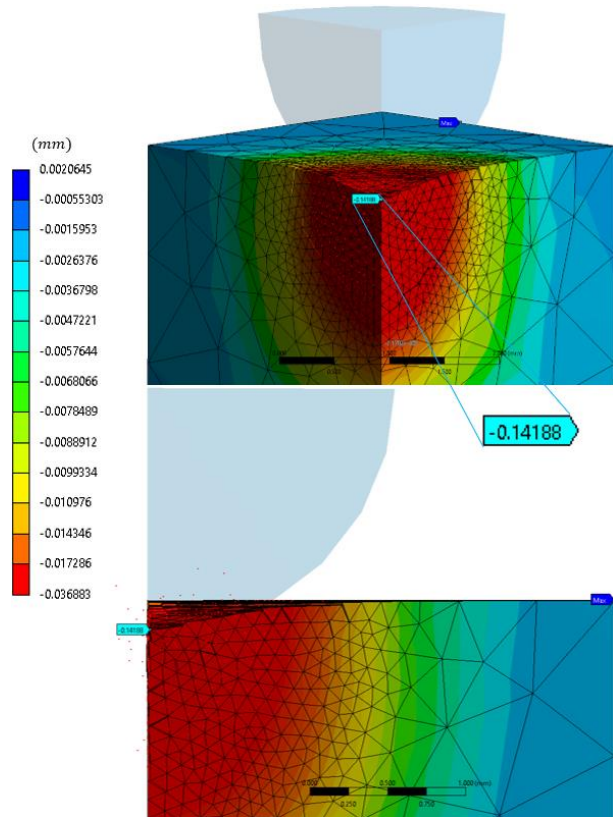


Fig 8: Deflection Due to Total (Minor + Major) Load (60kgf)

The deformations and deflections depicted in Fig. 8 follow the same basic principles discussed in Fig. 7. The initial point of contact between the indenter and specimen is where most deformations occur. It is also the location at which the maximum deflection occurs. Since the major load is added to the minor load, in this

To finish the FEA simulation of the RHT, the major load was removed from the applied load. With the minor load still in place, the depth recovery of the aluminum specimen was analyzed. As shown in Fig. 9, removing the major load resulted in a small upward displacement of the specimen's indentation. This

reduction in indentation depth is attributed to the elastic properties of aluminum. Although a majority of the indentation has undergone plastic deformation, a small section did not permanently deform. Instead, those parts underwent elastic deformation, constituting complete deformation recovery upon removal of the inducing load. This phenomenon hints at a possible correlation between the hardness of a material and its yield strength. Since the minor load is constantly held, full elastic recovery is not achieved by the specimen. Instead, the indentation depth is measured after partial elastic recovery, with the minor load still in place. Based on the explicit dynamic FEA simulation, the final deflection after removing the major load was 0.10517 mm in the downward direction. This value, coupled with the datum, will be used to calculate the permanent deflection of the aluminum specimen caused by the major load's addition.

With all of the deflection values recorded, Eq. (1) can be used to calculate the *RHN* as determined by the FEA simulation solutions. Table 2 summarizes the results.

TABLE II
FEA SIMULATION RESULTS

Datum Depth	0.061645 mm
Final Depth	0.10517 mm
Permanent deflection, <i>h</i>	0.043525 mm
Steel Ball Indenter Constant, <i>E</i>	130
Rockwell Hardness Number, <i>RHN</i>	108

By subtracting the datum depth from the final depth, the permanent deflection, *h*, of the aluminum specimen is found. Dividing the permanent deflection by 0.002 mm removes the units and normalizes the value. Subtracting the normalized permanent deflection from the steel ball indenter constant, *E*, results in a *RHN* of about 108. Therefore, the FEA simulation resulted in a *RHN* of scale H of 108 *HRHS*.

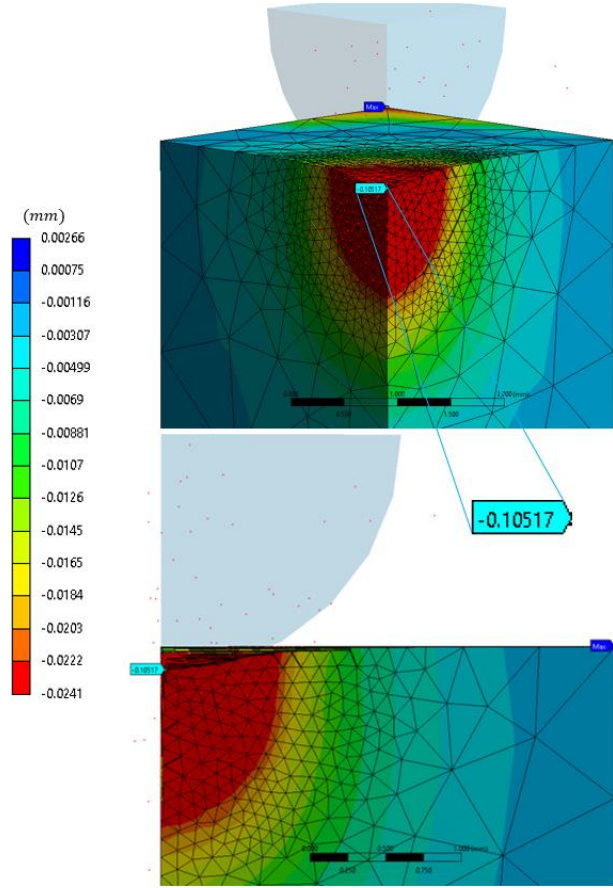


Fig 9: Deflection Due to Minor Load, After Removal of Major Load (10kgf)

C. Discussion

When comparing the experimental RHT to the FEA simulation, it can be seen that the FEA solution resulted in a larger *RHN*. The FEA solution predicted a final *RHN* that is 6 units larger than the experimental test. Possible reasons for the difference in hardness are rooted in several places. For the experimental test, the aluminum specimen surfaces were not prepared as well as they could have been. For instance, the specimen surface's surface could have been processed further to ensure that no minor irregularities exist. The larger the deformities on the surface, the larger the error will be in the *RHN* reading. For this reason, errors could have introduced to the physical experiment.

Since the FEA simulation uses numerical methods for determining the deflections, the final solution will always be an approximation. Based on how well the solution residuals converge, a more accurate solution can be calculated. Errors in the FEA simulation could also have originated because "broken" elements were used in the manual calculation of the *RHN*. Although the probe function was able to pick up on the deflections

quite easily, uncertainties persist. Additionally, the mesh used in the model could be further improved. Mesh refinement could be expanded further on the aluminum specimen, and the inflation radius could be extended to cover a larger area. The number of nodes and elements could also be increased by decreasing the average size of the elements. Experimenting with the order and type of elements used could also improve the FEA simulation's accuracy.

Engineers have tabulated empirical data on the hardness of aluminum in industry and researchers. Since data for the *RHN* of scale H of aluminum is hard to find, the *RHN* of scale B for aluminum was used and converted to scale H. Conversion between Rockwell hardness scales is a common practice, so conversion tables have been formulated. According to the literature, the *RHN* of aluminum on scale B is 60 *HRBS*. Using this value with the Rockwell hardness scale conversion table, the *RHN* of aluminum on scale H is about 108 *HRHS*. Comparing this with the experimental and FEA simulation results indicates that both results compare fairly with that of empirical data. Table 3 compares the results in more detail, marking the completion of Task 3.

TABLE III
ROCKWELL HARDNESS NUMBER RESULTS

	<i>Theoretical</i>	<i>% Error</i>
<i>Experimental Test</i>	102	5.56%
<i>FEA Simulation</i>	108	0.00%

V. CONCLUSIONS

A. Summary

To reinforce critical thinking and to problem-solve in engineering, aluminum's mechanical behavior was put under investigation. More specifically, RHT was studied and practice through actual experimental testing. FEA was then used to construct a simulation of the experimental model using numerical analysis. Not only does this encourage students to build a simple explicit dynamic FEA simulation, but it also gives them a real experiment that they can conduct and compare the results to by themselves. After extracting and calculating the *RHN* of both the experimental test and FEA simulation, the results were compared with tabulated data as made available by the industry and research.

B. Outcome

The experimental RHT resulted in *aRHN* on scale H of 102 *HRHS* for aluminum. The FEA simulation provided the datum and final deflection depths of the

indenter that were used to manually calculate a *RHN* of 108 *HRHS* for the aluminum specimen. According to empirical data on the hardness of aluminum, the theoretical *RHN* on scale H of aluminum is 108 *HRHS*. Based on the findings, the experimental test had an error of about 5.56%. The FEA simulation resulted in *aRHN* on-par with the theoretical hardness; the error of the FEA simulation was virtually nonexistent. Overall, the results fell in line with the expected hardness number of aluminum.

C. Future Work

Since the FEA simulation performed so well, future work suggestions are only considered for the experimental test. To improve the RHT results' accuracy, it is recommended to prepare the aluminum specimen more appropriately. If possible, the aluminum specimen should be uniform on composition and free of any and all irregularities. This includes cuts, holes, scratches, notches, and any other deformity. Additionally, it is recommended that students perform more than one hardness test on the same specimen to extract a complete estimation of the specimen's true hardness. With more than one experimental *RHN*, the values can be averaged so that the influence of random outliers are minimized. The larger the data set, the better the results should be.

ACKNOWLEDGEMENT

This research was partially supported by the Office of Research and Technology Transfer at the University of Texas at Tyler (Grant No. 21001333).

REFERENCES

- [1] W. Leslie, *The Physical Metallurgy of Steels*, New York: McGraw-Hill. (1981).
- [2] ISO 6506-1., *Metallic Materials - Brinell Hardness Test - Part 1: Test Method*, International Standard, Geneva, Switzerland. (2005).
- [3] ASTM E10-18., *Standard Method for Brinell Hardness of Metallic Materials*, ASTM International, West Conshohocken, PA. (2018).
- [4] F. Knoop, C. Peters and W. Emerson., *A Sensitive Pyramidal-Diamond Tool for Indentation Measurements*, *Journal of Research of the National Bureau of Standards*. (1939).
- [5] R. Smith and G. Sandland., *An Accurate Method of Determining the Hardness of Metals, with Particular Reference to Those of a High Degree of Hardness*, *Proceedings of the Institution of Mechanical Engineers*. 1 (1922) 623-41.
- [6] ISO 6507-1., *Vickers Hardness Test - Part1: Test Method*, International Standard, Geneva, Switzerland. (2005).

- [7] ASTM E384., Standard Test Method for Knoop and Vickers Hardness of Materials, ASTM International, West Conshohocken, PA. (2011).
- [8] R. Budynas and J. Nisbett., Shigley's Mechanical Engineering Design, New York, NY: McGraw-Hill Education. (2015).
- [9] Shanghai Shanghai Testing Machine Co., Ltd: 560RSS Digital Twin Rockwell Hardness Tester, [Online]. Available: http://sh-test.cc/product_18_560RSSDigitalTwinRockwellHardnessTester.html. [Accessed 20 April, 2019].
- [10] ASTM E18-19., Standard Test Method for Rockwell Hardness of Metallic Materials, ASTM International, West Conshohocken, PA. (2019).
- [11] G. Dai, K. Herrmann and F. Menelao., Two Approaches for Enhancing the Accuracy of the Rockwell Hardness Test, Measurement Science and Technology. 20 (2009).
- [12] M. Barmouz, K. Abrinia, and J. Khosravi., Using Hardness Measurement for Dislocation Densities Determination in FSPed Metal to Evaluation of Strain Rate Effect on the Tensile Behavior, Materials Science & Engineering A, 553 (2012) 917-19.
- [13] R. Perez-Bustamante, D. Bolanos-Morales, J. Bonilla-Martinez, I. Estrada-Guel, and R. Martinez-Sanchez., Microstructural and Hardness Behavior of Graphene-Nanoplatelets/Aluminum Composites Synthesized by Mechanical Alloying, Journal of Alloys and Compounds. 615 (2014) 578-82.
- [14] B. Kozola and Y. Shen., A Mechanistic Analysis of the Correlation Between Overall Strength and Indentation Hardness in Discontinuously Reinforced Aluminum, Journal of Materials Science. 23 (2003) 901-7.
- [15] S. Martin and H. Hynek., Mechanical Properties Determination of Unknown and 10Ch2MFA Steel Based on Non-Destructive Interumented Hardness Test, Key Engineering Materials. 662 (2015) 73-6.
- [16] P. Victor, P. Catalin, V. Mihai, V. Ionelia, S. Elena-Manuela, and P. Doru., Finite Element Method for Simulating the Vickers Hardness Test, Applied Mechanics and Materials. 419(24) (2014) 555.
- [17] W. Rule., Finite Element Modeling of Brinell and Rockwell Hardness Testing of Metals, Problems Involving Thermal-Hydraulics, Liquid Sloshing, and Extreme Loads on Structures. 489(2004).
- [18] C. Wei and J. Yang., A Finite Element Study on the Hardness of Carbon Nanotubes-Doped Diamond-Like Carbon Film, Journal of Materials Research. 27(1) 2012.
- [19] R. Ekici, M. Apalak, M. Yildirim, and F. Nair., Simulated and Actual Micro-Structure Models on the Indentation Behaviors of Particle Reinforced Metal Matrix Composites, Materials Science and Engineering A. 606 (2014) 290-8.
- [20] Rockwell Hardness Test., Gordon England, [Online]. Available: <https://www.gordonengland.co.uk/hardness/rockwell.htm>. [Accessed 20 April, 2019],
- [21] Shihabudheen Kunnath, Mohammed Irfan K, Mohammed Nasarudheen P, Mohammed Nishad C, Muhammed Faris T., Study of Mechanical Properties and Micro structure of the Composition Al7075/Al2O3 Metal Matrix Composites, SSRG International Journal of Mechanical Engineering. 6(6) (2019) 3-6.

BIOGRAPHY



Dr. Chung-Hyun Goh is an Assistant Professor in the Department of Mechanical Engineering at The University of Texas at Tyler. He has a PhD in Mechanical Engineering from Georgia Institute of Technology. His interests include the areas of robotics and computer-aided integrated design and manufacturing. He is currently working on Medical Device design and machine learning applications in Engineering. His teaching interests include design, robotics, and system dynamics and control.



Mr. Armin Yazdanshenas is a recent graduate from The University of Texas at Tyler where he earned his Master of Science in Mechanical Engineering. He also has a bachelor's degree in Mechanical Engineering from Mississippi State University. In his academic career, he has conducted both undergraduate and graduate research. His interests include mechanical design, fluid-structure interaction, and convolutional neural networks.